Research Article | Vol. 27, No. 8 | 15 Apr 2019 | OPTICS EXPRESS A257
Optics EXPRESS

Evaluation and measurement of heliostat misalignment in solar power plant using vector model

E. CARRETERO,[1,2,*] J. PRECIADO,[2,3] I. SALINAS,[2,3] I. AYORA,[2,3] AND C. HERAS[2,3]

[1]*Departamento de Física Aplicada, Universidad de Zaragoza, C/Pedro Cerbuna, 12, Zaragoza 50009, Spain*
[2]*Grupo de Tecnologías Fotónicas, Instituto de Investigación en Ingeniería de Aragón (I3A), Universidad de Zaragoza, Zaragoza 50001, Spain*
[3]*Departamento de Ingeniería Electrónica y Comunicaciones, Universidad de Zaragoza, C/ Maria de Luna, 1, Zaragoza 50018, Spain*
[*]*ecarre@unizar.es*

Abstract: Heliostat alignment evaluation is among the main issues in solar tower concentration plant operation and maintenance. This paper describes a novel method used to evaluate heliostat misalignment and its experimental verification. This method provides a different way of visualizing beam centroid pointing errors by generating the complete deviation curve for each axis. This, for example, would be useful for verifying a heliostat's correct alignment by using a measurement performed out of the receiver target, using these traces to calculate its reflection's expected location, given a known misalignment. This measurement could be performed during operation simply by including a reflective element in the heliostat and two detector arrays on the tower's surface. This model has been tested for various types of misalignments of a heliostat at different hours, dates, and heliostat locations. The simulation results have been validated by using an experimental setup at a scale of 1:100.

1. Introduction

Central receiver solar power plants generally implement open loop control for the tracking system of heliostats to ensure that the light they reflect will continuously converge on the receiver area [1]. One of the main influential factors in the global efficiency of concentrating solar power technology is the total power directed over the course of a day to the receiver. Pointing errors cause a drift of the concentrated beam, which moves away from its ideal trajectory, directly diminishing power plant performance [2].

Due to the relevance of this effect, several simulation methods to predict the tracking error of a single heliostat based on information about its geometrical errors have been presented in [3,4]. In [5], Jones and Stone shows the calculated positions of the heliostat beam on the target at 1-hour increments, implementing fixed values for three main types of geometric error sources: encoder reference offset, mirror alignment and heliostat tilt. In [6], Díaz-Felix et al simulated tracking errors by adding an angular deviation angle to the vector normal to the heliostat, in azimuth or elevation, relative to its ideal orientation. Numerical results are also shown, illustrating daily drift trajectories for a fixed value of the deviation angle. In [7], Guo et al introduces a simulation model of sun-beam traces over the target plane for an azimuth–elevation tracking heliostat, also considering fixed geometric error sources. Other models as [6] introduce Montecarlo distributions to predict random deviation error values over the course of the day. Usually, these kind of simulations evaluate the impacts of geometric errors on the tracking accuracy of the reflection beam considering only the ray reflected at the center of the heliostat for a fixed geometric error. Because of that, each trace

#351545 https://doi.org/10.1364/OE.27.00A257
Journal © 2019 Received 12 Nov 2018; revised 4 Jan 2019; accepted 8 Jan 2019; published 20 Feb 2019

Optics EXPRESS

evaluates only a particular heliostat error condition, and the evolution of the tracking error with the magnitude of the geometric error is not directly illustrated.

In this paper we evaluate, instead of a single ray, the two sets of rays that would be reflected from the center of the heliostat for different values of its alignment error. One set of rays belongs to azimuthal errors and the other to elevation errors. This kind of simulation provides a better understanding of the relationship between tracking error curves evolution and geometric error values, and their limits can be directly established for each heliostat location. Furthermore, the resultant curves can be useful to evaluate performance and errors in closed-loop control of central receiver that use the reflection of solar light in the heliostat plane [8,9].

2. Description

We define the geometric error in the alignment of a heliostat as the angular difference between the real and ideal vectors normal to the plane of the heliostat. This error originates mainly from three different sources in the tracking and the mechanical structure of the heliostats: encoder reference offset error, mirror alignment error and heliostat tilt error [10,11]. This alignment error is put on display in the curve traced on the target plane by the central solar ray reflected on the mirror surface, when it is evaluated over the course of a single day. In absence of errors, this curve would collapse to a single point.

In this paper, we calculate the evolution of the tracking error as a function of the geometric error. We achieve that by tracing the two sets of rays reflected by the heliostat towards the central tower when considering different values of elevation and azimuthal geometric errors.

In order to generate these sets of rays, we place two cylindrical mirror surfaces at the location of the heliostat. One of them, coaxial to the elevation-rotating axis of the heliostat, produces the rays reflected for different elevation errors. The other, with its axis orthogonal to the elevation axis and parallel to the heliostat surface plane, generates the rays reflected for every azimuthal error. The position and curvature radius of these cylinders depend on the type of error to be analyzed, as described below.

As an example, Fig. 1 illustrates the cylindrical surface for elevation geometric error in the case of a reference offset error in an encoder. It shows in the elevation plane view, three positions of the heliostat mirror, $H(\varepsilon_i)$, when it is deviated in an angle ε_i from the ideal position. For this type of error, the cylinder center is at the rotation point of the heliostat (point C) and its radius r is the distance to the center of the heliostat. The cylindrical surface is the envelope of the positions $P(\varepsilon_i)$ of the heliostat center for all the range of elevation error values ε_i. Therefore, vectors $n(\varepsilon_i)$ normal to this surface are also vectors normal to the heliostat when it is rotated an angle ε_i. As will be described later in the simulation model, each pair of values $(P(\varepsilon_i), n(\varepsilon_i))$ of the cylindrical surface defines a point of reflection of the incident sun-beam and results in a ray reflected towards the receiver plane. This model can be extended to the other two sources of error (mirror misalignment and heliostat tilt), as will be described later.

Optics EXPRESS

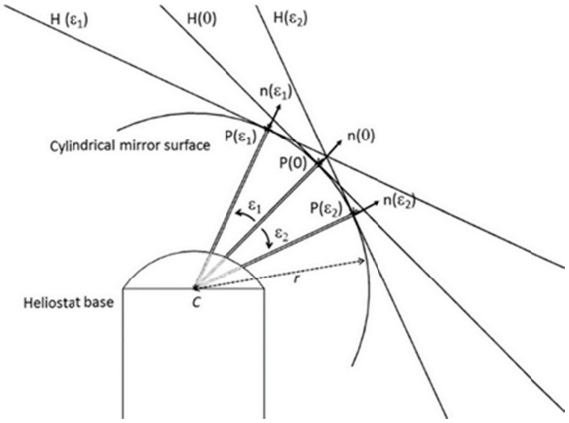

Fig. 1. Cylindrical surface for the error in the elevation of an heliostat.

The same description is valid for the set of rays generated due to azimuthal geometric error. The cylindrical surface $\left(P(\phi_i), n(\phi_i)\right)$ will be the envelope of the positions $P(\phi_i)$ of the center of the heliostat for different azimuthal error values ϕ_i. The two cylindrical surfaces for elevation and azimuth geometric errors are shown together in Fig. 2. The $n(0,0)$ vector represents the ideal orientation, with no geometric error.

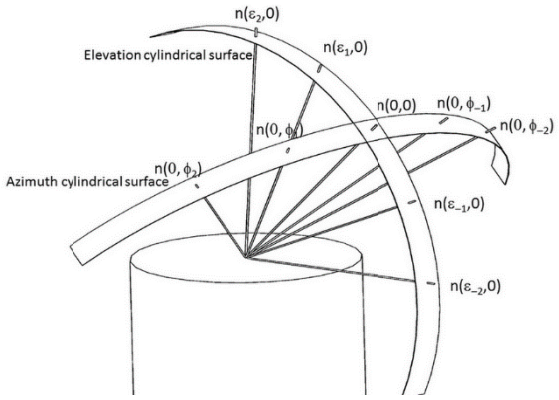

Fig. 2. Cylindrical surfaces for the error in elevation and azimuth of a heliostat.

The 4-mrad divergence solar rays are reflected by the cylindrical mirror and result in a cone of rays traveling towards the target. Each ray is generated by a pair $\left(P(\varepsilon_i, \phi_i), \hat{n}(\varepsilon_i, \phi_i)\right)$. The incidence of this cone of rays on the tower surface traces a curve on it. Depending on the orientation of the tower plane with respect the direction of the cone of rays, this projection curve will be a different conic section, the parameters of which will vary throughout the day.

In order to detect the beams generated by the cylinders the real system should have two arrays of detectors placed on the receiver plane. As these arrays can be located outside the target, the detectors will not be exposed to the high temperatures at target.

Although in our model we calculate the reflection on cylinders, the real setup could consist of rotating polygonal mirrors. These rotating prisms generate a reflected beam similar to that generated by a cylinder, but the reflected light is modulated at a certain frequency depending on the rotation speed of the prism. This makes possible the measurement of the radiation from each prism simultaneously and independently, simply by using different rotation frequencies as labels.

Optics EXPRESS

3. Theoretical model

In order to simulate the evolution of the tracking error as a function of the geometric error, it is necessary to calculate every single ray reflected by two perpendicular cylindrical surfaces. Those rays depend on the position of the sun, the position of the concentrator, and the position of the heliostat. The former is obtained from the declination angle δ and the hour angle ω, indicating the sun elevation angle above the ground and the rotation from north to east respectively. Thus, we can define a solar vector $\vec{S}$ [12,13]:

$$\vec{S} = \left(S_x, S_y, \mathrm{S}_z\right) = \left(\cos\delta\cos\omega, -\cos\delta\sin\omega, \sin\delta\right). \tag{1}$$

The center of the receiver target in the tower will be the origin of our local coordinate system, where the X-axis is perpendicular to the target plane, Y-axis is parallel to the tower face and Earth's surface and the Z-axis is perpendicular to the Earth's surface (Fig. 3).

$$O = \left(x_o, y_o, z_o\right) = (0,0,0) \tag{2}$$

This local coordinate system may not match, depending on the orientation of the tower, the coordinate system used to describe the solar vector $\vec{S}$. In this case, we must transform the solar vector $\vec{S}$ to the local coordinate system, using rotation matrices relative to each axis.

$$T_x(\alpha) = \begin{pmatrix} 1 & 0 & 0 \\ 0 & \cos(\alpha) & -\sin(\alpha) \\ 0 & \sin(\alpha) & \cos(\alpha) \end{pmatrix}, \tag{3}$$

$$T_y(\beta) = \begin{pmatrix} \cos(\beta) & 0 & \sin(\beta) \\ 0 & 1 & 0 \\ -\sin(\beta) & 0 & \cos(\beta) \end{pmatrix}, \tag{4}$$

$$T_z(\gamma) = \begin{pmatrix} \cos(\gamma) & -\sin(\gamma) & 0 \\ \sin(\gamma) & \cos(\gamma) & 0 \\ 0 & 0 & 1 \end{pmatrix}, \tag{5}$$

where $T_x(\alpha)$ describes a rotation of an angle α around the X-axis. $T_y(\beta)$ and $T_z(\gamma)$ are the same for the other two axes.

Following Eq. (5), we can transform the solar vector $\vec{S}$ to our local coordinate system $\vec{S}_{local}$ using the angle between the tower and the North direction φ.

$$\vec{S}_{local} = T_z(\varphi)\vec{S} \tag{6}$$

Optics EXPRESS

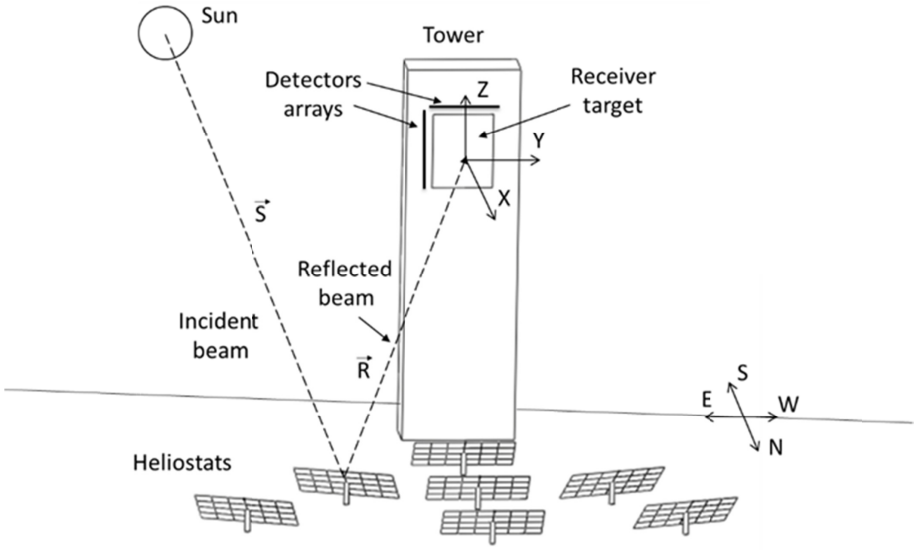

Fig. 3. Local coordinate system.

The position of the heliostat C in this local coordinate system is defined as the position of the rotation center of the heliostat Eq. (7). However, the surface of the heliostat rotates around that point with a certain radius. $\vec{r}$ will be the vector that connects the rotation center to the center of the surface of the heliostat Eq. (8).

$$C = (x_C, y_C, z_C) \tag{7}$$

$$\vec{r} = (r_x, r_y, r_z) \tag{8}$$

Then, the position of the center of the mirror, P, will be:

$$P = (x_P, y_P, z_P) = (x_C, y_C, z_C) + (r_x, r_y, r_z). \tag{9}$$

The vector $\vec{n}$, normal to the mirror surface, will have the same orientation of $\vec{r}$, thus:

$$\vec{n} = \frac{\vec{r}}{\|\vec{r}\|} = (n_x, n_y, n_z) \tag{10}$$

A vector formulation of the law of reflection Eq. (11) gives us the reflected ray vector $\vec{R}$ according to the incident ray vector $\vec{I}$ and the normal to the reflective surface $\vec{n}$. In the case we are studying, the incident vector will be the solar vector $\vec{S}$ in the local coordinate system $\vec{I} = \vec{S}_{local}$.

$$\vec{R} = \vec{I} - \frac{2\vec{I}\cdot\vec{n}}{\|\vec{n}\|^2}\vec{n} = (R_x, R_y, R_z) \tag{11}$$

Using Eqs. (9) and (11), we can estimate the projection of the reflected rays over the concentrator plane (x = 0) for any heliostat orientation.

$$\begin{cases} Y = y_p - R_y \dfrac{x_P}{R_x} \\ Z = z_p - R_z \dfrac{x_P}{R_x} \end{cases} \tag{12}$$

Equation (12) calculates the projections of both real and virtual reflected rays. Only real rays will actually reach the plane YZ (x = 0) after being reflected by the heliostat, so we have to make sure that the sign of x_P is opposite to that of R_x.

We can now calculate the projection of the reflected ray for any vector normal to the heliostat. Our first aim is to obtain the vector normal to the heliostat in absence of elevation or azimuthal errors ($\vec{n}(0,0)$ in Fig. 2). To calculate this vector, we have to determine the reflected vector that hits the center of the concentrator O. This vector $\overline{R}_P$ is the one that connects the center of the mirror P to the center of the concentrator O:

$$\vec{R}_P = \left(R_{Px}, R_{Py}, R_{Pz}\right) = O - P = \left(x_0, y_0, z_0\right) - \left(x_P, y_P, z_P\right) = \left(x_0, y_0, z_0\right) - \left(x_C, y_C, z_C\right) - \left(r_x, r_y, r_z\right). \tag{13}$$

Equation (13) can be used to calculate the reflection vector for any position P of the center of the heliostat. Now, we can calculate the normal vector of the heliostat that causes the reflected ray to impact on the center of the solar concentrator $\vec{n}(0,0) = \vec{n}_P$ using the vector reflection law Eq. (11) and $\overline{R}_P$:

$$\vec{S} - \frac{\vec{R}_P}{\left\|\vec{R}_P\right\|} = \frac{2\vec{S}\cdot\vec{n}_P}{\left\|\vec{n}_P\right\|^2}\vec{n}_P = \lambda\vec{n}_P. \tag{14}$$

Since we only need to know the direction of the normal vector $\vec{n}_P$, it is not necessary to calculate λ. However, we have to take into account that $\vec{R}_P$ depends on the vector $\vec{r}$ shown in Eq. (13), and the vector $\vec{r}$ is related to the normal vector $\vec{n}$ as shown in Eq. (10). Therefore, Eq. (14) becomes:

$$\lambda\left(n_{Px}, n_{Py}, n_{Pz}\right) = \frac{\lambda}{\left\|\vec{r}\right\|}\left(r_x, r_y, r_z\right) = \left(S_x, S_y, S_z\right) + \frac{\left(x_C, y_C, z_C\right) + \left(r_x, r_y, r_z\right)}{\sqrt{\left(x_C + r_x\right)^2 + \left(y_C + r_y\right)^2 + \left(z_C + r_z\right)^2}}. \tag{15}$$

This expression is difficult to solve, but can be simplified. Vector $\vec{r}$ in the right side can be neglected because it has the same direction as $\vec{n}$ and will only affect the value of the scalar λ, and $\|\vec{r}\|$ is much smaller than the distance of the heliostat to the concentrator.

$$\lambda'\left(n_{Px}, n_{Py}, n_{Pz}\right) \simeq \left(S_x, S_y, S_z\right) + \frac{\left(x_C, y_C, z_C\right)}{\sqrt{\left(x_C\right)^2 + \left(y_C\right)^2 + \left(z_C\right)^2}} \tag{16}$$

Although the approximation error is small, it can be further reduced with an iterative calculation of the normal vector:

$$\lambda'_i\vec{n}_{Pi} = \frac{\lambda'_i}{\left\|\vec{r}\right\|}\vec{r}_{Pi} = \vec{S} - \frac{\vec{R}_{i-1}}{\left\|\vec{R}_{i-1}\right\|}, \tag{17}$$

where i is the number of the iteration, and

$$\vec{R}_0 = \left(x_0, y_0, z_0\right) - \left(x_C, y_C, z_C\right). \tag{18}$$

Optics EXPRESS

Given a sun vector $\vec{S}$, a heliostat located at point C and a target located at the origin of coordinates O, Eqs. (16) and (17) approximate the value of $\vec{n}_P$. Successive iterations provide a very good approximation to the exact value.

Using this model, once the ideal normal vector is known, the deviation of the beam at the plane of the tower can be calculated as a function of the misalignment of the heliostat. That is, we can add an error to the ideal normal vector in either of the two directions (elevation or azimuthal) and then calculate the reflected ray with the reflection vector law Eq. (11) and its projection on the plane of the tower Eq. (12).

These misalignments cause the center of the heliostat to travel over a cylindrical surface as shown in Figs. 1 and 2. If we calculate the reflection on a cylindrical surface, instead of a heliostat, the result will be a conic section on the plane of the solar tower. This curve is an useful representation of the effects on the heliostat suffers of geometrical errors like encoder reference offset, mirror alignment or heliostat tilt, because each point of the curve will belong to the ray reflected with the matching normal vector of the cylinder (Fig. 1).

4. Results

4.1 Simulations

Using the theoretical model in the previous section, we have developed our own simulation software to calculate the deviations as a function of misalignment. Figure 4 shows the results for six different locations of a heliostat. Figure 4 shows the curves generated by the reflection of a collimated beam (sun) on two perpendicular cylindrical surfaces when they are perfectly aligned (when both curves pass through the center of the receiver target). The results are shown for different times of the day and six different locations of heliostats.

The plane of the heliostat is replaced by two cylinders perpendicular to each other. The reflection on the vertical cylinder (red) projected on the tower is the locus of the rays reaching the tower when the heliostat has an elevation misalignment, and the horizontal cylinder (blue) is the same for deviations in azimuth. If there is no misalignment, the reflected ray will be at the center of the concentrator. Three curves for each cylinder represent the projections at 8, 12 and 16 hours, showing their evolution over the course of a day.

These graphs reveal the importance of the heliostat location in the impact of possible misalignments. Similar results could be obtained using the calculations of [6] and adding not a single but a set of angular deviation angles. However, the effect of cylinder radio is not taken into consideration in that work, and the inclusion of two cylindrical surfaces makes possible a better understanding of the effect of geometrical errors.

Moreover, the knowledge of the complete deviation curve could have interesting applications. For example, it would be possible to verify the correct alignment of a heliostat with a measurement performed out of the concentrator, using this traces to calculate the expected location of its reflection given a known misalignment.

Although Fig. 4 is useful to see how the sun beams would deflect according to the angular deviation of the heliostat, it could also be interesting to know the effect of a particular angular error during a day. For this purpose, another set of simulations have been performed. Figure 5 shows the variation of the reflected rays throughout a day for different angular deviations. As before in Fig. 4, the heliostat has been replaced by two perpendicular cylinders in order to simulate azimuthal and elevation errors. Each graph represents a different location for the heliostat. As expected, the effect of the same angle deviation is lower for the heliostats near the tower(Figs. 5(a)-5(c)) than the ones far from it (Figs. 5(d)-5(f)). For example, in Fig. 5(a) the spots remain inside the area of the concentrator for deviations up to 12mrad, whereas in Fig. 5(d), the limit is under 4mrad.

In addition, using these graphs we can determine the hours in which the beams are inside the receiver target. For example, in Fig. 5(b), an azimuthal error of 12mrad means that only at

Optics EXPRESS

16pm or before 8am the ray will hit the receiver target, this is deduced from the fact that only at this time the reflected beam is located inside the concentrator.

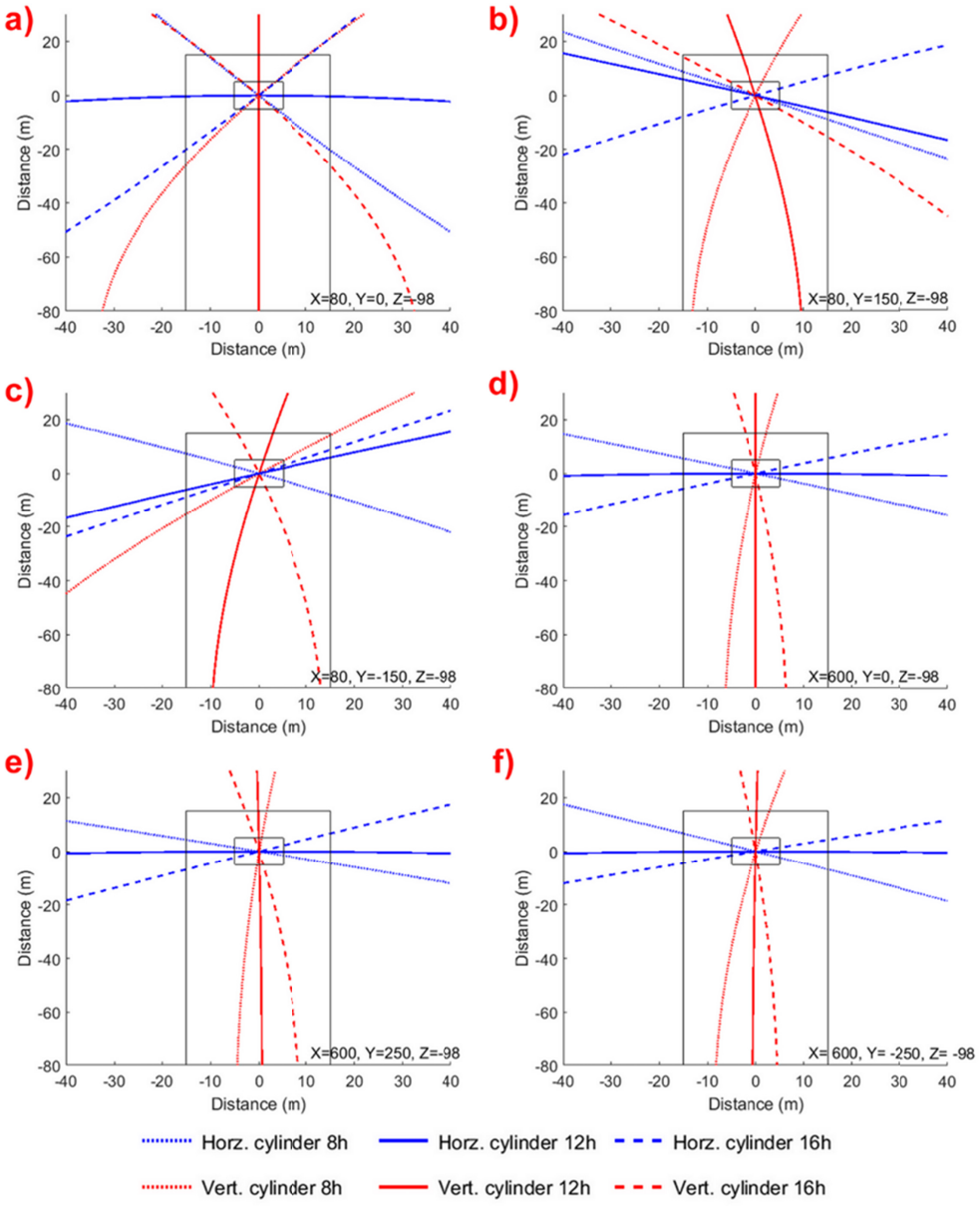

Fig. 4. Deviation curves for different hours (solar hour) and locations (placed on the lower right side of each graph in meters) of the heliostat (simulations for June 21).

Optics EXPRESS

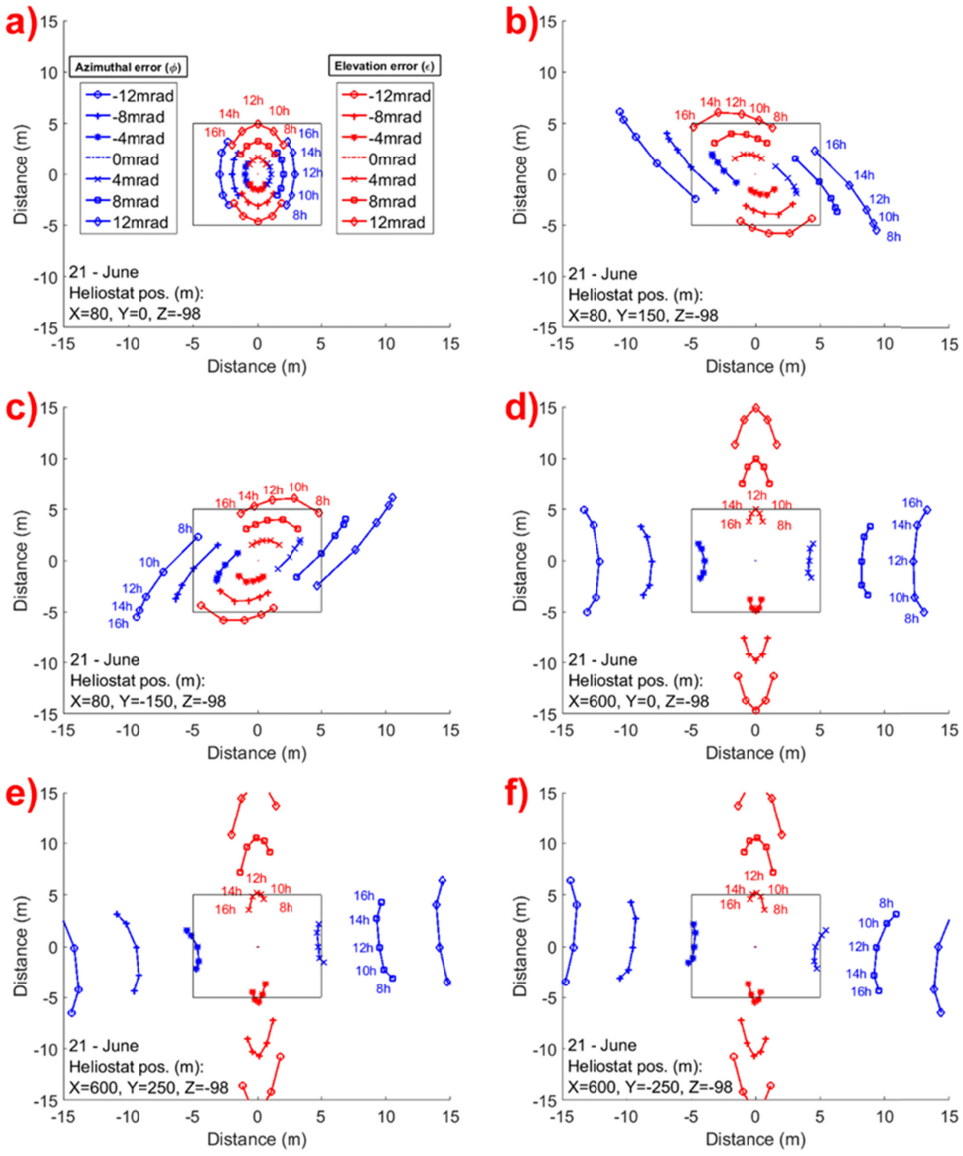

Fig. 5. Evolution of the deviation for different hours of the day as a function of errors in azimuth and elevation. Each graph belongs to a heliostat location on a certain date.

Using this method, we can calculate the deviation of the rays due to every possible source of misalignment (location of the heliostats, angular errors in alignment, solar time and date), separately or combined.

4.2 Experimental validation

In order to test the accuracy of the simulations we have built a 1:100 scale experimental setup (Fig. 6). The light source is a He-Ne laser with a beam expander providing a 10 mm diameter and 4 mrad divergence beam (aprox). The cylinder equivalent to the heliostat with all the range of possible elevation error values is replaced by a polygonal rotating mirror. This rotating mirror has a diameter of 35 mm and an height of 2 mm (the rotating mirror is not exactly scaled to the heliostat, but this has a minimal effect on the experiment). The light from the laser is reflected by this rotating mirror and results in a set of rays directed towards

the tower model. A calibrated screen is placed in this model to measure the trace formed by the reflection.

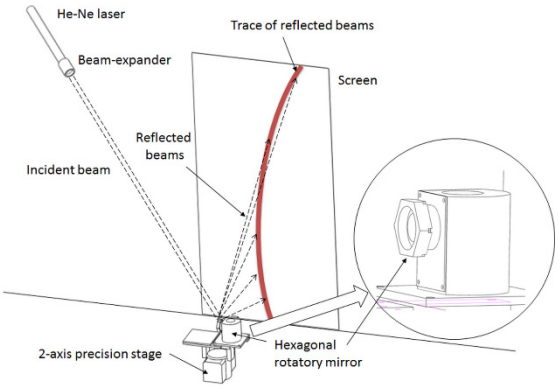

Fig. 6. Experimental setup.

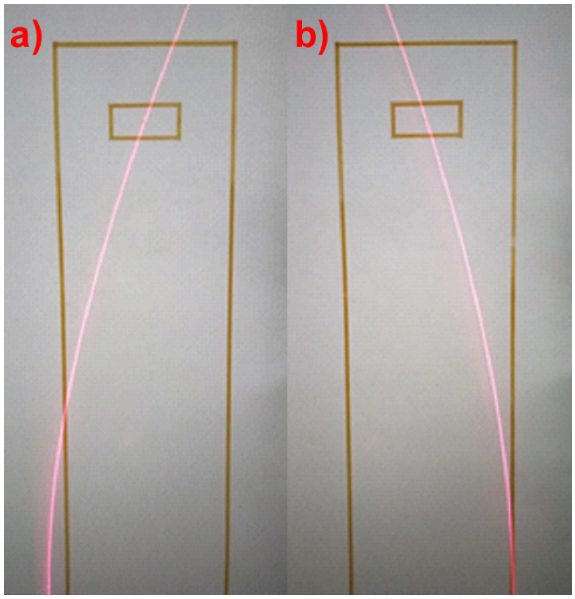

Fig. 7. Traces resulting from two different misalignment conditions in our experimental setup.

Figure 7 shows the traces on the screen for two given positions of the laser (sun) and the mirror (heliostat). In Fig. 7(a), the heliostat is located at X = 150cm, Y = –16cm, Z = –143cm while the sun-laser is at azimuth = 101° and elevation = 50° (as the scale is 1:100, centimeters in the experimental setup correspond to meters at real scale). In Fig. 7(b), the heliostat is located at X = 150cm, Y = –45cm, Z = –143cm and the laser is at azimuth = 260° and elevation = 48°. The locations of the mirror and the laser define the projections over the tower. In Fig. 7(a), the reflected rays trace a hyperbola with its focus at the left. Figure 7(b) is also a hyperbola, but the focus is at the other side.

Optics EXPRESS

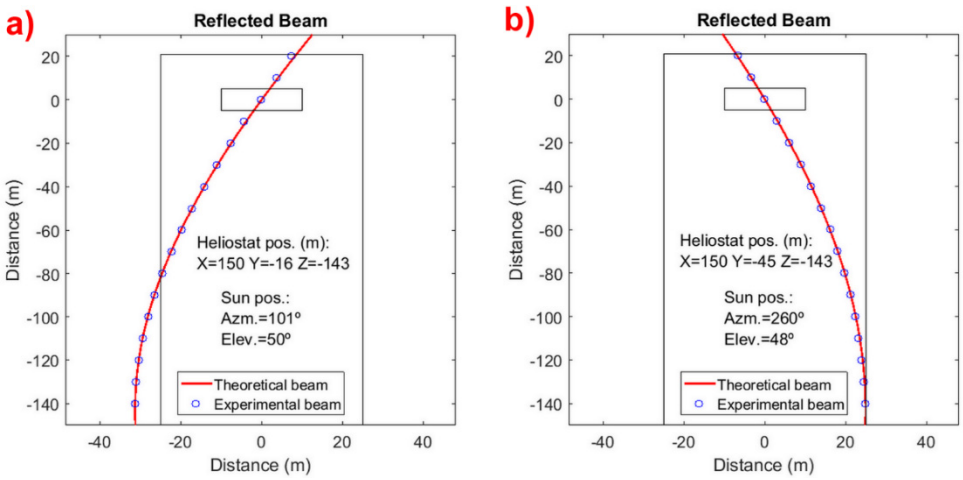

Fig. 8. Results of the experimental setup at 1: 100 scale versus the simulation results.

Figure 8 compares the experimental and simulated projections on a solar tower. There is a very good agreement between measurements and simulation, validating the model and approximations used in section 3.

4.3 Discussion

The use of reflective cylindrical surfaces (or equivalent polygonal surfaces) allows us to measure the misalignment of heliostats in positions away from the receiver target. In addition, the modulation of the reflected beam makes possible the simultaneous measurement of the misalignment of all the heliostats of a tower plant in real time. In heliostats with several mirrors, the installation of reflective surfaces for each mirror can be considered, though it would increase the cost of the system.

Using the curves generated in Fig. 4, we are able to know where the signal should cross the detector arrays when the heliostat is properly aligned, which gives us the information needed for a closed-loop system. In summary, if we know the cross points on the detectors arrays (target plane) of the curve generated by the reflector element, we can calculate the misalignment of the heliostat because we can calculate the cross points on the detectors arrays when the heliostat is perfectly aligned (for any position of heliostat or position of the sun).

5. Conclusions

We have developed a new model to evaluate misalignments in the orientation of the heliostats in solar tower power plants, using a vector calculation of the beam paths and replacing the full range of elevation and azimuthal errors by two perpendicular virtual reflective cylinders.

This model has been used in a simulation to evaluate the effect of different types of misalignments of a heliostat on the position of the reflected beam on the tower. This effect can be calculated for different hours, dates and heliostat locations, and for the complete range of deviations at the same time. In addition, the measurement system allows an experimental measurement of misalignment away from the solar concentrator and the design of a closed-loop system for heliostat control.

Funding

Spanish Ministerio de Economía y Competitividad (RTC-2016-5226-3); Gobierno de Aragón/European Social Fund (T20_17R).

Optics EXPRESS

Disclosures

The authors declare that there are no conflicts of interest related to this article.

References

1. C. K. Yang, T. C. Cheng, C. H. Cheng, C. C. Wang, and C. C. Lee, "Open-loop altitude-azimuth concentrated solar tracking system for solar-thermal applications," Sol. Energy **147**, 52–60 (2017).
2. W. Huang, P. Hu, and Z. Chen, "Performance simulation of a parabolic trough solar collector," Sol. Energy **86**(2), 746–755 (2012).
3. M. Coquand, F. Henault, and C. Caliot, "Backward-gazing method for measuring solar concentrators shape errors," Appl. Opt. **56**(7), 2029–2037 (2017).
4. Y. Yao, Y. Hu, S. Gao, G. Yang, and J. Du, "A multipurpose dual-axis solar tracker with two tracking strategies," Renew. Energy **72**, 88–98 (2014).
5. S. A. Jones and K. W. Stone, "Analysis of solar two heliostat tracking error sources," Tech. Rep. SAND99–0239C Albuq. Sandia Natl. Lab. (1999).
6. L. A. Díaz-Félix, M. Escobar-Toledo, J. Waissman, N. Pitalúa-Díaz, and C. A. Arancibia-Bulnes, "Evaluation of heliostat field global tracking error distributions by Monte Carlo simulations," Energy Procedia **49**, 1308–1317 (2014).
7. M. Guo, Z. Wang, and F. Sun, "Simulations of reflected sun beam traces over a target plane for an azimuth elevation tracking heliostat with fixed geometric error sources," Sol. Energy **97**, 102–111 (2013).
8. R. Alonso, C. Heras, J. Pelayo, I. Salinas, and J. Subias, "Closed-loop control system and method for heliostats in solar power towers," U.S. patent ES2558847 (A1) Abstract of corresponding document: WO2016005620 (A1) (February 9, 2016).
9. M. R. Convery, "Closed-loop control for power tower heliostats," in *High and Low Concentrator Systems for Solar Electric Applications Vi*, K. VanSant and R. A. Sherif, eds. (Spie-Int Soc Optical Engineering, 2011), Vol. 8108, p. 81080M.
10. H. Fathabadi, "Comparative study between two novel sensorless and sensor based dual-axis solar trackers," Sol. Energy **138**, 67–76 (2016).
11. W. Nsengiyumva, S. G. Chen, L. Hu, and X. Chen, "Recent advancements and challenges in solar tracking systems (STS): A review," Renew. Sustain. Energy Rev. **81**, 250–279 (2018).
12. J. A. Duffie and W. A. Beckman, *Solar engineering of thermal processes* (Wiley, 1991).
13. M. Guo, F. Sun, Z. Wang, and J. Zhang, "Properties of a general azimuth-elevation tracking angle formula for a heliostat with a mirror-pivot offset and other angular errors," Sol. Energy **96**, 159–167 (2013).